Condition Monitoring System: A Flexible Hybrid Electronics Approach for Sealed Container Applications

M. Panahi[1], A. J. Hanson[1, 2], D. Maddipatla[1], S. Masihi[1], B. B. Narakathu[2], B. J. Bazuin[1], S. Miller[3], M. Z. Atashbar[1]

[1]Department of Electrical and Computer Engineering, Western Michigan University Kalamazoo, MI, USA

[2]SafeSense Technologies, L.L.C. Kalamazoo, MI, USA

[3]NextFlex National Manufacturing Institute San Jose, CA, USA

ABSTRACT

A comparative study is presented between two advanced flexible hybrid electronics (FHE) monitoring systems designed for accurately measuring temperature within storage containers across various industries, including food, pharmaceuticals, agriculture, automotive, and defense. Flexible hybrid electronics involve the combination of novel printing processes and traditional electronic manufacturing processes, resulting in flexible devices with improved performance. The first system, a copper-flex system (CFS), employs an 88.9 μm polyimide substrate with 35 μm thick copper traces, coated with a 12.5 μm polyimide solder mask. The second system, a printed-flex system (PFS), utilizes a 127 μm polyimide substrate and screen-printed conductive silver ink. Both FHE systems use a 32-pin very thin quad flat no-lead (VQFN) package attached on a thin polyimide flexible substrate with high-temperature resistance and high-tensile strength. In both CFS and PFS, the VQFN is attached using Sn96.5/Ag3.0/Cu0.5 and Sn42/Bi57.6/Ag0.4 solders, respectively, from Chip Quik® (Ancaster, Ontario, Canada). After assembly, reliability and durability tests were conducted to validate the performance of the temperature sensor and the interconnections of the CFS and PFS prototypes. Further, environmental and mechanical characterizations including, moisture and insulation resistance, corrosion, elongation, bending, terminal bond strength, and peel tests were performed based on IPC-TM-650 and ASTM standards. Moisture and insulation resistance test on the PFS test coupons without a coating layer indicated stable resistance of approximately 18 MΩ, while permanent color change indicated oxidation of copper on uncoated CFS test coupons. After 72 hours of corrosion test, both the CFS and PFS "meander line" test coupons covered with polyimide showed negligible weight and resistance change of approximately 0.35%, and 0%, respectively. A Young's modulus of 7.17 GPa and 2.6 GPa was calculated from the elongation test for the CFS and PFS, respectively. Bending tests on PFS revealed negligible average resistance change (0.1%) during 180° bending cycles, while no impact was recorded on the CFS system. During the terminal bond strength test, soldered wires detached from the CFS test coupons at an average force of 43 N, while it was 3.8 N on the PFS test coupons. Both systems with polyimide coating layer demonstrate robustness and reliability for diverse applications in various industries.

Key words: Temperature sensor; asset monitoring system; copper flexible system; printed flexible system; flexible hybrid electronics.

INTRODUCTION

Condition monitoring of tangible assets often entails the utilization of a hardware and software system that records, transmits, stores, and processes information on ambient conditions by using various sensors, data communication technologies, and software algorithms. Condition monitoring systems have found widespread applications across various industries, including automotive, defense, food, and medical industries, for several decades [1-5]. However, the full potential of such systems remains largely untapped in applications that necessitate miniaturized and conformal structures with flexible and thin form factors.

For instance, in agricultural storage applications, there is a need for flexible and lightweight condition monitoring systems to monitor the moisture, temperature, and other environmental conditions of seeds and plants [6]. One other example of a condition monitoring application is in healthcare and logistics. Asset monitoring systems can track the location and condition of vaccine storage containers during transportation. This helps pharmaceutical industries optimize logistics operations and prevent damage or loss of vaccines. For example, during the COVID-19 pandemic, Pfizer-BioNTech produced large quantities of vaccines that had to be transported and stored worldwide at temperatures between 2 °C to 8 °C for up to a month [7].

In addition to vaccines and perishable food items like meat and fruit [8], the US Department of Defense (DoD) emphasizes the importance of condition monitoring for ammunition in a thin and flexible form factor [9]. Precise temperature monitoring during transportation and storage, either long or short-term, is vital to maintain the effectiveness of sensitive items. Temperature changes can result in vaccine wastage, food spoilage, ammunition degradation, or even fatalities, underscoring the need for continuous and accurate condition monitoring. Traditional monitoring systems are often rigid and made using electronic fabrication techniques. However, the market needs lightweight, compact, thin, affordable, and flexible monitoring systems tailored to various applications, especially for monitoring conditions inside containers. Therefore, developing such systems is crucial for the global economy and public health, as they ensure the safe condition of assets in different types of containers.

Flexible hybrid electronics involve the combination of novel printing processes and traditional electronic manufacturing processes, resulting in flexible devices with improved performance [10-22]. In this work, two advanced FHE based condition monitoring systems are designed and fabricated for monitoring temperature inside a DoD-relevant ammunition container (M2A2). A comparative study is performed between a CFS and PFS prototype, which are both based on popular manufacturing processes in FHE. The systems were designed to meet the DoD accepted requirements, in terms of performance and dimension [9]. The capability of the CFS and PFS were tested to monitor temperature from - 20°C to +60°C with an accuracy of ±1°C, while maintaining a battery life of over 3 years. In addition, the capability of the sensor-readout circuit interconnect was examined to withstand a bending radius of 0.8 mm and 30 opening and closing cycles of the container lid. Additionally, the PFS and CFS test coupons were tested and compared for performance and reliability under varying environmental and mechanical effects based on IPC-TM-650 and ASTM standards.

EXPERIMENTAL

A. Design and Fabrication

The CFS and PFS circuits were designed with Altium® Designer software (a registered trademark of Altium Limited, San Diego, California, USA). The overall dimensions of the CFS and PFS prototypes are shown in Fig. 1(a). The main components of the CFS and PFS include microcontroller unit (MCU), temperature and humidity sensor, quartz crystal, voltage regulator, joint test action group (JTAG) port, microSD™ (a trademark of SD-3C, LLC, Redmond, Washington, USA) card port, battery, and battery header connector (Fig. 1(b)). The microSD™ card was positioned at the bottom of the substrate and stiffeners were used to handle any associated stress. The JTAG port is on the top left and can be removed after programming to reduce the overall height. The HDC2022 sensor from Texas Instruments (Dallas, Texas, USA) offers high-accuracy temperature and relative humidity (RH) measurement, with ratings of ±0.2°C and ±2% RH, respectively. Additionally, the sensor is IP67-rated [23] for water and dust protection and features low power consumption. The sensor was positioned at the end of an interconnect, separated from the circuit. This allows the sensor to be placed inside a sealed container while keeping other components outside, making data collection easier and without affecting the container's internal environment. The quartz crystal ECS-33B is placed next to the MCU in the middle of the circuit, to provide the clock signal. A 32-pin VQFN microcontroller unit (CC2640R2FRSMT) from Texas Instruments reads sensor responses, monitors battery levels, and activates visual indicators. In addition, it writes data to the microSD™ card, and uses real-time clock to sleep/wake up. Low-dropout voltage regulator (TPS70612DBVT from Texas Instruments) controls the microSD™ card voltage to minimize any potential data loss. A flexible and thin lithium battery (CP142828, 1.4×29×29 mm) with 150 mAh capacity from GMBPOW® (a registered trademark of Guangzhou Markyn Battery Co., Ltd., China) was used to power the CFS and PFS. A Molex Pico-Ezmate crimp/header connector (Lisle, Illinois, USA) was used for battery connection due to its reliability and ease of use. The key materials employed in the fabrication of CFS and PFS prototype are summarized in Table S1 (Supporting Information).

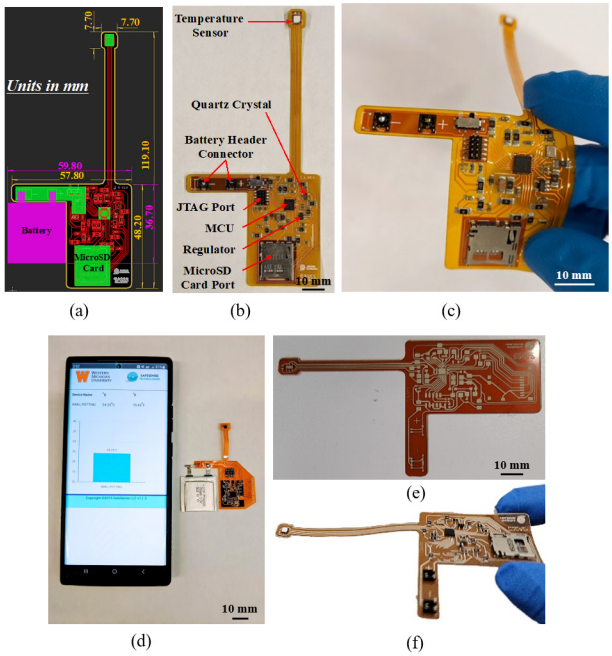

Figure 1: (a) CFS and PFS layout dimensions, (b) fabricated CFS prototype with soldered component, (c) flexible CFS prototype, (d) wireless CFS with Android™ app, (e) printed PFS, and (f) fabricated PFS prototype.

The CFS prototype PCBs were fabricated by depositing copper traces with a thickness of 35 µm onto a 88.9 µm thick polyimide flex substrate. These copper traces were deposited through the wet etching method. The polyimide substrate was then covered with a yellow overlay solder mask with a thickness of 12.5 µm. The surface finish used was Electroless Nickel/Immersion Gold (ENIG). The photograph of the flexible CFS prototype is shown in Fig. 1(c). The maximum thickness of the CFS at the microSD™ card port location

was approximately 1.95 mm. Figure 1(d) shows the CFS prototype equipped with a thin-film battery and connected wirelessly via Bluetooth® (a registered trademark of Bluetooth Special Interest Group, Kirkland, Washington, USA) to an Android™ (a trademark of Google LLC, Mountain View, California, USA) application interface. However, this prototype remained unused as it did not comply with DoD requirements, which mandated data recording solely on a microSD™ card.

For the fabrication of the PFS, a stainless-steel screen with a mesh count of 325 threads per inch (TPI), emulsion thickness (MS-22) of 15 µm, ultra-thin wire diameter of 22.8 µm, and deflection angle of 22.5° was obtained from Microscreen LLC (South Bend, Indiana, USA). Conductive silver ink (DuPont™ 5025) from DuPont™ (a trademark of DuPont de Nemours, Inc. Wilmington, Delaware, USA) was then deposited on a Kapton® 500 HN substrate (Kapton® is a registerd trademark of DuPont de Nemours, Inc., Wilmington, Delaware, USA). This was accomplished using an HMI MSP 485 screen printer (Lebanon, New Jersey, USA) with an offset height of 1 mm. Following this, the printed samples were cured in an Accutemp 09S vacuum oven from Across International (Livingston, New Jersey, USA) at 120 °C for 8 minutes to evaporate the solvent. The photographs of the PFS prototype are shown in Fig. 1(e) and (f). It is clearly visible that the conductive traces have been successfully deposited without any overlap. The printed PFS prototypes were then accurately cut out using a Graphtec FC8600 plotter (Yokohama, Kanagawa, Japan) as shown in Fig. S1. Following this, solder paste (Chip Quik® Solder Sn42/Bi57.6/Ag0.4) was applied to the PFS and components were attached prior to heating in the advanced Puhui T-937 reflow oven (from Taian Puhui Electric Technology Co., Ltd, Taian, Shandong, China) as shown in Fig. S2.

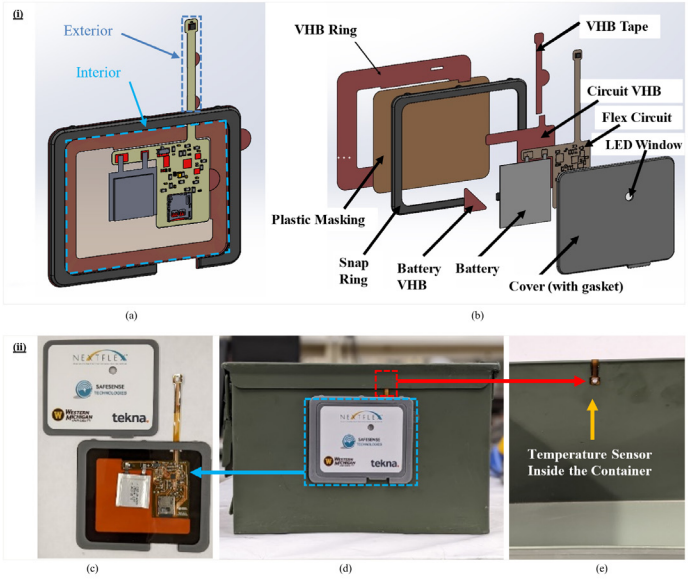

Figure 2: Snap-in enclosure: (i) illustration: (a) schematic, and (b) exploded view; (ii) fabricated prototype: (c) fabricated CFS with designed enclosure, (d) installation of enclosure on the container, and (e) installation the sensor inside the container.

The soldering challenges encountered with PFS components are detailed and illustrated in the supporting information and Fig. S3. In addition, CTFC-12 Konform® Flexcoat Conformal Coating from Chemtronics® (a registered trademark of Chemtronics, Kennesaw, Georgia, USA) and polyimide tape from Bertech® (a registered trademark of Bertech Corporation, Torrance, California, USA) company were used as a coating layer on the PFS samples.

The enclosure was designed based on several critical specifications, including the overall thickness of the device, the capacity to resist water ingress in accordance with the IP64 specification [24]. In addition, the design provides access to a microSD™ card through an open/close tab while being protected from water ingress. Figures 2(i) and 2(ii) illustrate the snap-in enclosure design and fabricated prototype, respectively. The top cover snaps into place inside the outer ring when pressed down, and can be easily removed by lifting an included tab. The enclosure was attached to the container using a double-sided 3M® VHB 5907 adhesive tape (3M® is a registered trademark of 3M Company headquartered in St. Paul, Minnesota, USA). As depicted in Fig. 2(i)(a) and (b), the flex circuits (PFS or CFS) were attached to a plastic mask (Kapton® 500 HN substrate) and enclosed inside the snap ring of the enclosure using 3M® VHB 5907 adhesive tape. A top cover was 3D printed using an acrylonitrile butadiene styrene (ABS) filament and features a foam gasket (ethylene propylene diene monomer (EPDM) closed-cell foam) which seals against water ingress when compressed. Acrylonitrile butadiene styrene provides a good balance of strength, flexibility, and necessary resistance to water, humidity, salt spray, and withstands -20°C to 60°C temperatures. A polycarbonate transparent plastic was 3D printed on the top cover to facilitate visual access to the LED indicators. Finally, a die-cut thin plastic sheet provides masking around the edge to give the foam gasket a non-adhesive surface to seal. The system was designed to meet the requirements for performance in the temperature range of -20 °C to 60 °C and have these dimensions: The interior portion (electronic readout module and battery) has a thickness of < 3.175 mm and an area of < 645.16 mm2. The exterior portion (sensor and interconnect) has a thickness of <3.175 mm and an area of < 2580.64 mm2. Table S2, summarizes the materials employed in the fabrication of the enclosure prototype, and Table S3 outlines potential materials for utilization in large-scale production.

To meet the IPC-TM-650 standards for environmental and mechanical characterizations, three test coupons ("dogbone" [Fig. 3(i)(a)], "comb pattern" [Fig. 3(i)(b)], and "meander line" [Fig. 3(i)(c)] were designed using AutoCAD® software (a registered trademark of Autodesk, Inc., San Francisco, California, USA). The designs and dimensions of the test coupons are shown in Fig. 3(i), and photographs of the fabricated CFS and PFS coupons are shown in Fig. 3(ii).

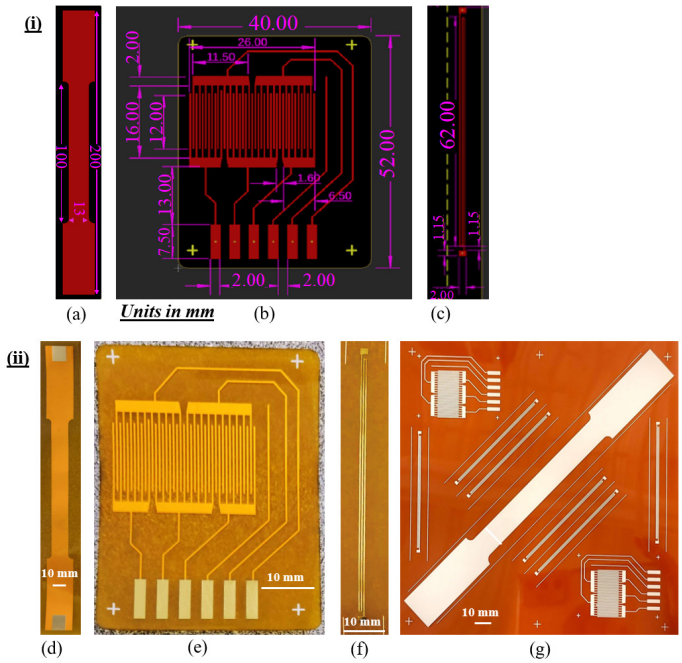

Figure 3: Test coupons: (i) CAD designs: (a) dogbone, (b) comb pattern, and (c) meander line; (ii) fabricated test coupons: (d) CFS dogbone, (e) CFS comb pattern, (f) CFS meander line, and (g) PFS test coupons.

B. Test Methods

Surface Morphology

Surface topology and the material composition of the printed samples were characterized using Bruker Contour GT-K white light interferometer (Billerica, Massachusetts, USA) and JEOL (Tokyo, Japan) scanning electron microscope (SEM).

Environmental Tests

The initial test involved the functional test to evaluate the temperature sensor's performance. Subsequently, the effects of moisture and insulation, and corrosion were investigated in accordance with IPC-TM-650-2.6.3 - Class H and ASTM E-595 test standards, respectively. The equipment utilized in these tests included a Traceable® 6511 data logging thermometer certified by the National Institute of Standards and Technology (NIST) (Traceable® is a registered trademark of Control Company, Friendswood, Texas, USA), and the Thermotron® SE-3000 environmental chamber (Thermotron® is a registered trademark of Thermotron Industries, Holland, Michigan, USA). In addition, a Fluke® 101 digital multimeter (Fluke® is a registered trademark of Fluke Corporation, Everett, Washington, USA), and a Citizen® CY204 laboratory balance scale (Citizen® is a registered trademark of Citizen Holdings Co., Ltd., Nishi-Tokyo, Tokyo, Japan) were used for measuring the resistance and weight of the test coupons. Furthermore, a Keithley 6517A Electrometer (Solon, Ohio, USA) was used for measuring the high resistances of the "comb pattern" test coupons.

In functional test, the temperature sensor was characterized for various temperatures by placing the CFS and the thermometer inside the environmental chamber, as shown in Fig. 4. The sensor responses were recorded against the highly accurate Traceable® thermometer (±0.1 °C) to calibrate the sensor across different relative humidity levels, ranging from 20% RH to 80% RH, in steps of 20%.

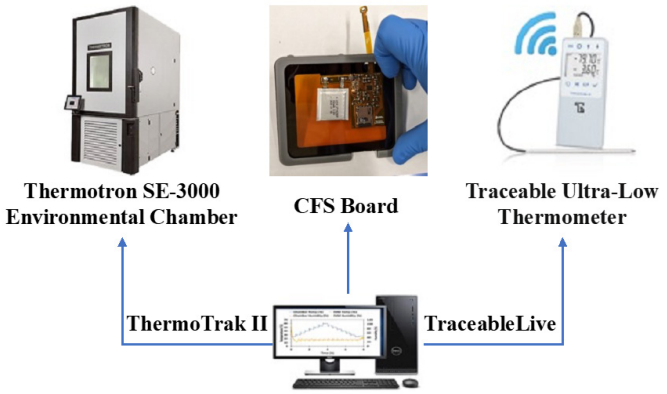

Figure 4: Experiment setup for the sensor calibration.

In order to test the moisture and insulation resistance, the CFS and PFS "comb pattern" test coupons with and without encapsulant coating were initially crimped with connecting wires. Following this, the test coupons were placed inside the chamber, and a bias voltage of 10 VDC was applied to the test coupons. The chamber temperature was then varied from 25 °C to 65 °C while maintaining a relative humidity of 90% RH for 20 cycles. Each temperature ramp (increased from 25 °C to 65 °C and decreased from 65 °C to 25 °C) was programmed to run for time duration of 2.5 hours while the temperature of 65 °C was maintained for 3 hours. Hence, the completion of 20 cycles of moisture and insulation resistance tests required a total duration of 160 hours.

To investigate the corrosion effect, the CFS and PFS "comb pattern" and "meander line" test coupons were placed inside a pail and exposed to a corrosion material under a controlled temperature and humidity environment, as depicted in Fig. 5. Sulfur (S) powder and saturated potassium nitrate (KNO3) solution were used to provide the corrosion exposure and constant relative humidity, respectively. A 40 mm × 10 mm blower fan from Anvision® (a registered trademark of Anvision Technology (Beijing) Co., Ltd. Beijing, China) was used to circulate air inside the pail. The pail setup was placed inside the environmental chamber and its temperature and relative humidity were set to 60 °C and 80% RH, respectively.

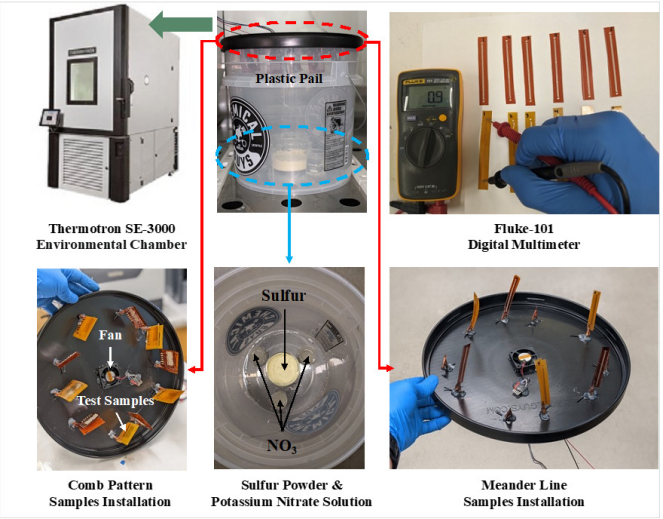

Figure 5: Experiment setup for the corrosion test.

Mechanical Tests

The mechanical testing sequence commenced with a durability test. Elongation, bending, terminal bond strength, and peel resistance were subsequently investigated as per the IPC-TM-650 2.4.18.1; IPC-TM-650, 2431-1; IPC-TM-650, 2.4.20; and ASTM D1876 standards, respectively. Mechanical tests were performed by using an Instron® 4301 tester and a Mark-10® ESM301 motorized test stand integrated with a force gauge machine (Instron® and Mark-10® are registered trademarks of Instron Corporation, based in Norwood, Massachusetts, and Mark-10 Corporation, located in Copiague, New York, respectively). A GW Instek 6100 precision LCR meter (New Taipei City, Taiwan) and a C# custom-developed software were used for recording the resistance variations.

In durability test, the effect of opening and closing the container lid on the interconnect of the CFS and PFS prototypes was examined. This investigation aimed to comprehend the durability of the copper and silver traces within the interconnect. The CFS and PFS prototypes with and without encapsulant coating was attached to the M2A2 container and connected to a GW Instek 6100 precision LCR meter (Fig. 6(a)). The CFS and PFS systems were on the front side/exterior of the container and the interconnect was bent over the lip of the container and attached to the interior wall of the container (Fig. 6(b)). After that, the lid of the container was opened and closed 30 times and the effect of the stress/damage that occurs on the interconnect was investigated by recording the resistance across the interconnect (Fig. 6(c)).

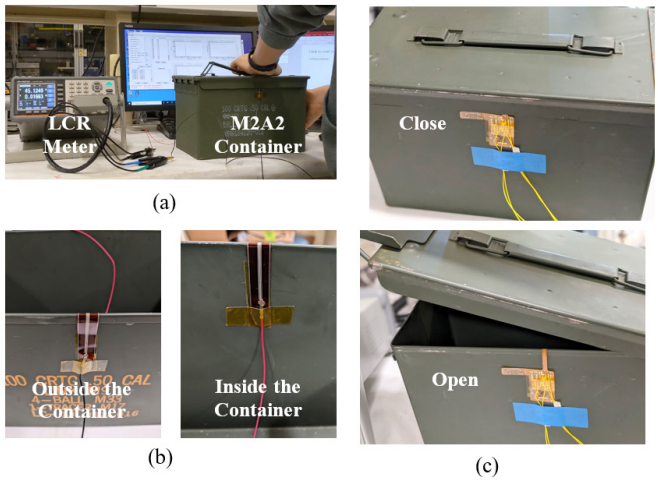

Figure 6: Durability test: (a) experiment setup, (b) inside and outside view of the container with PFS test coupon, (c) opening and closing the container lid.

Elongation test was performed using CFS and PFS "dogbone" test coupons, as per the IPC-TM-650 2.4.18.1, shown in Fig. 7(i) (a) and (b). The specimen was loaded between the clamps of an Instron® 4301 tensile tester, and the clamps were programmed to elongate the coupon at a speed rate of 0.5 mm/min [Fig. 7(i)(a)]. As the clamp elongated the test coupon, the copper or silver traces along with polyimide film were subjected to strain, which in turn created fracture leading to the tearing of the coupon [Fig. 7(i)(b)]. Elongation test was employed to extract the Young's modulus (E), which quantifies a material's stiffness, and is expressed as the ratio of stress (σ) to strain (ε). Young's modulus can be computed using Eq. (1):

$$E = \frac{Stress}{Strain} = \frac{\sigma}{\varepsilon}\ (Pa) \qquad (1)$$

Where, stress is the force (F) applied per unit area (A) and can be calculated using Eq. (2):

$$\sigma = \frac{F}{A}\ (Typically\ N/m^2\ ,\ or\ Pa) \qquad (2)$$

The area (A) is determined by multiplying the thickness and width of the specimen, measured in square meters (m^2). Stress is typically measured in Newtons per square meter (N/m^2), also known as Pascals (Pa). Strain is a measure of deformation, representing the displacement between particles in the material. Strain is calculated as the change in length (ΔL) divided by the original length (L_0) using Eq. (3):

$$\varepsilon = \frac{\Delta L}{L0} \qquad (3)$$

In bending test, the "meander line" test coupon was mounted between the moving and stationary clamps of a Mark-10® test stand and the force gauge as shown in Fig. 7(ii)(c). The bonded wires of the test coupon were connected to a GW Instek 6100 precision LCR meter and a custom developed software was used for recording the resistance variations across the conductive traces during the 100-cycle bend tests [Fig. 7(ii)(d)]. The "meander line" test coupon was then subjected to a cyclic bend test, where copper and conductive printed silver traces on the specimen were bonded to wires (using crimp connectors) and subjected to a 180° bend test which is repeated for 100 cycles.

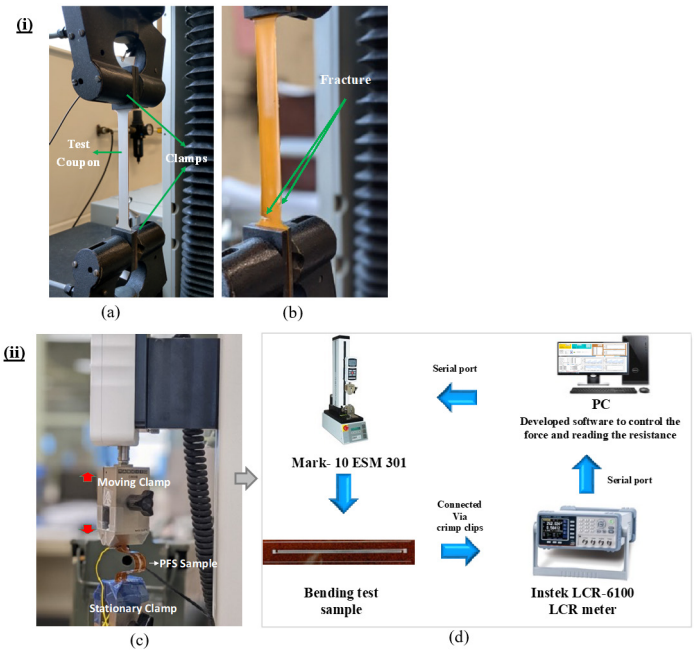

Figure 7: (i) Elongation test: (a) dogbone test coupon placed between the tensile tester clamps, and (b) fracture on test coupon; (ii) bend test: (c) meander line test coupon subjected to bending, and (d) experiment setup for bending test.

In terminal bond strength test, the terminal pad on the PCB was bonded to a wire with length of 5 cm using a traditional 60W soldering device and an Alpha Fry rosin core solder wire (tin/lead -60/40) (Elizabeth, New Jersey, USA) [Fig. 8(i)(a)]. The sample was placed on the Mark-10® test stand and the free end of the bonded wire was attached to the vertically movable clamp. The bonded wire was pulled at a rate of 50 mm/min with the movable clamp and the force required to remove/detach the wire was recorded using the force gauge of the Mark-10® test stand [Fig. 8(i)(b)].

Peel test was performed to investigate the adhesion strength of the double-sided adhesive tape used for attaching the CFS/PFS to the enclosure and subsequently to the container, as shown in Fig. 8(ii)(c) and (d). This was completed in accordance with the ASTM D1876 standard, by attaching a 127 mm long 3M® VHB 5907 adhesive tape to the ammunition container. The container was cut into small strips, enabling the uniform attachment/detachment of the adhesive to/from the container. The ammunition container strips were held between two static clamps; while the adhesive attached to the container was held between two vertically movable clamps of the Instron® 4301 tester via a polyimide film, as shown in Fig. 8(ii)(c). The clamps holding the Kapton® film attached to the adhesive were programmed to move vertically at a rate of 254 mm/min and the corresponding forces required to peel off the adhesive were recorded by the tester. A similar test was repeated by replacing the polyimide film with the ABS pieces (Note: ABS was used to make the enclosure) [Fig. 8(ii)(d)].

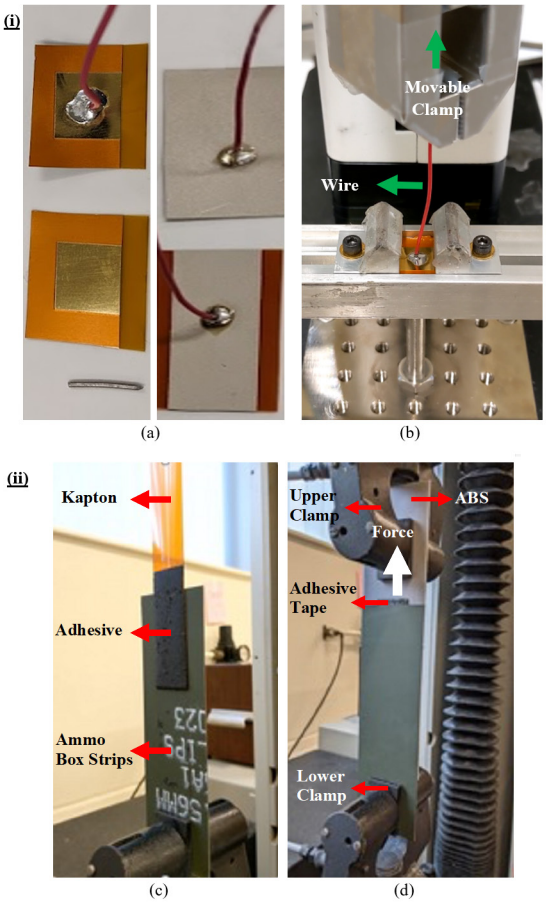

Figure 8: (i) Terminal bond strength test: (a) soldering on terminal pad, and (b) soldered wire attached to the movable clamp; (ii) peel test: ammunition container strips with adhesive and (c) Kapton®, and (d) ABS placed between the Instron® 4301 tester clamps and peeling off the adhesive from the container.

RESULTS AND DISCUSSION

Surface Morphology

In this characterization, a thickness of 10.50 ± 0.10 µm and roughness of 1.48 ± 0.03 µm was measured for the printed samples, as shown in Fig. 9(a) and (b), respectively. From the SEM image shown in Fig. 9(c), it is evident that the silver film is homogeneously printed, and the silver flakes are uniformly spread without any cracks. The cross-sectional view of the printed film with encapsulant clearly shows the uniform deposition of encapsulant (with thickness of 48.60 ± 0.30 µm) on the printed film (Fig. 9(d)).

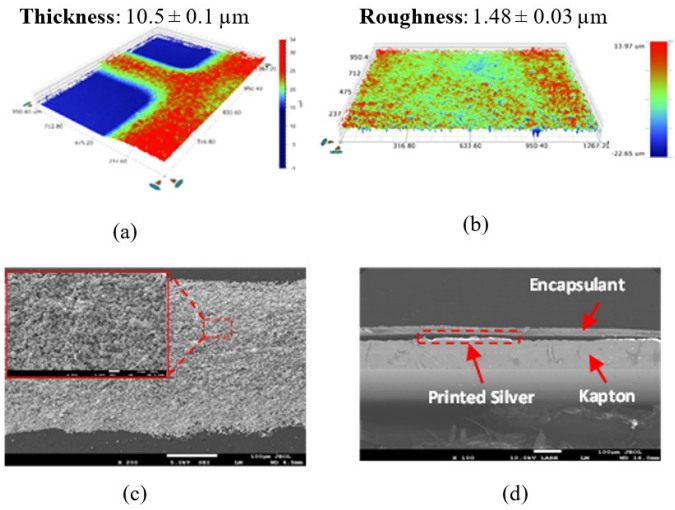

Figure 9: Surface morphological characterization of PFS: (a) thickness, and (b) roughness, (c) high magnification SEM image of printed silver and (d) cross-sectional SEM image of encapsulant on printed traces of Kapton®.

Environmental Tests

During the functional test to evaluate the performance of the sensor, the temperature of the chamber was continuously increased stepwise from -20 °C to 60 °C (in steps of 2 °C and step time of 15 minutes) and responses of the thermometer and the sensor response were recorded. As shown in Fig. 10, the sensor response was matched with the thermometer and is linear from -20 °C to 60 °C, with a correlation factor of almost unity. This calibration graphs and its equations were used in the programming code of the MCU to calibrate the response read by the temperature sensor for different humidity ranges to increase the accuracy.

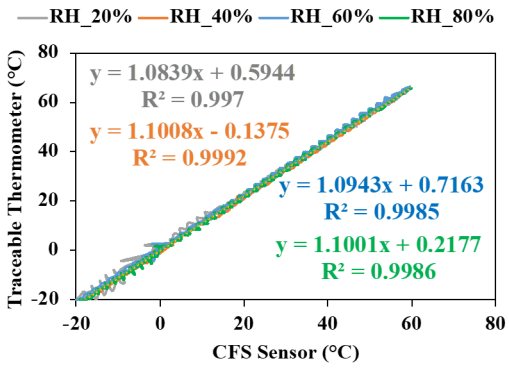

Figure 10: Calibration curve and equations in different RH%.

The effect of humidity on the sensor performance was investigated by varying RH levels from 20% RH to 80% RH, in steps of 20%. Initially, at 20% RH step, the temperature of the chamber was increased from -20 °C to 60 °C, and then decreased to -20 °C, in steps of 2 °C, with a step time of 15 minutes (Fig. S4). The responses of the temperature and humidity sensor (ST), thermometer (TT) and chamber (CT) were recorded. This same temperature sweep was repeated at different relative humidity levels (40% RH, 60% RH, and 80% RH), and the temperature and humidity responses were recorded. It was observed that temperature and humidity sensor clearly follow the temperature and humidity variations in the chamber.

In moisture and insulation resistance test, the resistance of the PFS and CFS samples with and without encapsulant coating was measured every 24 hours and was found to be stable at ≈ 18 MΩ for coated CFS (Fig. 11(a)), coated and uncoated PFS test coupons (Fig. 11(b)) which is also reported in our previous work [21]. On the other hand, CFS test coupons without solder mask experienced resistance shift (Fig. 11(a)) and permanent change in color that can be attributed to the oxidation of copper [Fig. 11(c) and (d)]. This clearly shows that coating layer plays a significant role to protect the copper from oxidation while printed silver layer has not been affected by the moisture and temperature variations.

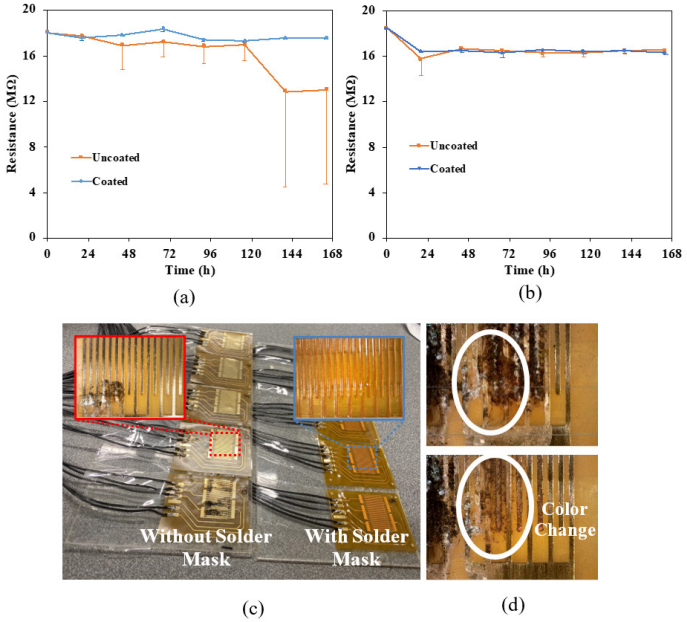

Figure 11: Moisture and insulation resistance test: (a) CFS resistance response, (b) PFS resistance response, (c) CFS comb pattern test coupons with and without solder mask, and (d) color change of CFS after IPA cleaning.

After the completion of the corrosion test, the "meander line" test coupons' weight change was measured as 0.35 ± 0.03% after 72 hours for both coated CFS and uncoated CFS samples (Fig. 12(a)). Similarly, the PFS samples covered with a polyimide tape (from Bertech® company) exhibited a maximum weight change of 0.33 ±IPC 0.02% whereas PFS samples uncoated and coated with Chemtronics® CTFC-12 exhibited a weight change of 0.95 + 0.27% (Fig. 12(b)). The maximum relative resistance changes of "meander line" test coupons' was measured as ≈ 0% for coated CFS, uncoated CFS, and coated PFS with a polyimide tape, while it was measured as 367.75 ± 32.35% for uncoated PFS. The maximum relative weight change of the CFS "comb pattern" test coupons'

after 144 hours was measured as 0.26 ± 0.03% and 0.34 ± 0.07% for coated and uncoated samples, respectively. Similarly, the weight change was measured as 0.37 ± 0.10% and 0.83 ± 0.04% for the samples coated with Chemtronics® CTFC-12 and uncoated PFS "comb pattern" test coupons, respectively. This clearly indicates that the CFS samples (both coated and uncoated) and coated PFS samples were not affected by sulfur vapors or high humidity and temperature, and resisted against corrosion unlike uncoated PFS samples. The microscopic images of the CFS and PFS samples are shown in Fig. S5. No visible corrosion was observed on the copper traces of both coated and uncoated samples ((Fig. S5(a) and (b)). Although the uncoated PFS samples exhibited corrosion (as depicted in Fig. S5(c)), those coated with polyimide remained unaffected by corrosion [illustrated in Figure S5(d) and (e)]. In addition, pictures show that polyimide has provided a better protection against corrosion when compared to Chemtronics® CTFC-12 spray coat (Fig. S5(e)).

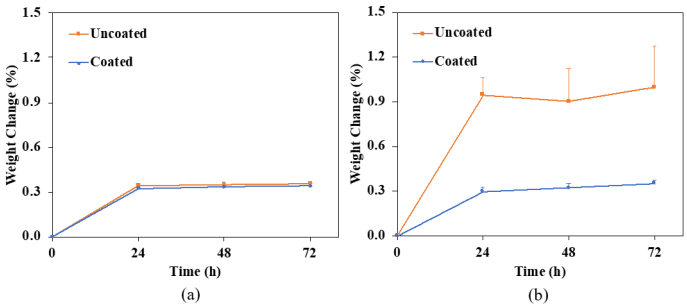

Figure 12: Corrosion test, meander line test coupons' weight change: (a) CFS, and (b) PFS.

Mechanical Tests

In durability test, the lid of the container was opened and closed 30 times (Fig. 13(a)) resulted in an average resistance change of 0.16 ± 0.08% and 0.13 ± 0.05% for the coated and uncoated CFS samples (Fig. 13(b)). This clearly shows a very minimal impact on the interconnect lines of CFS.

Similarly, a PFS resistance change of 3 ± 0.35% and 24 ± 1.85% was measured for the prototypes that were coated with Chemtronics® CTFC-12, as well as for the uncoated samples, respectively, when opening and closing the lid after 30 cycles (Fig. 13(c)). The average resistance change clearly shows that there is very minimal impact of the container lid on the interconnect lines coated with encapsulant when compared to uncoated samples. Similar results were observed when examining the coated and uncoated samples using microscopic and SEM images. As shown in Fig. S6(a) and (b), the microscopic images of coated sample clearly show that there was no visible damage to the silver traces under the encapsulant and silver nanoflakes were strongly attached to the polyimide substrate even after the test. However, the microscopic and SEM images of the uncoated samples clearly indicate the damage sustained by the printed traces and detachment of silver nanoflakes from the polyimide substrate [Fig. S6(c) and (d)]. High magnification images (Fig. S6(d)) revealed the impressions of the container on the silver nanoflakes of the areas where the silver particles were partially detached.

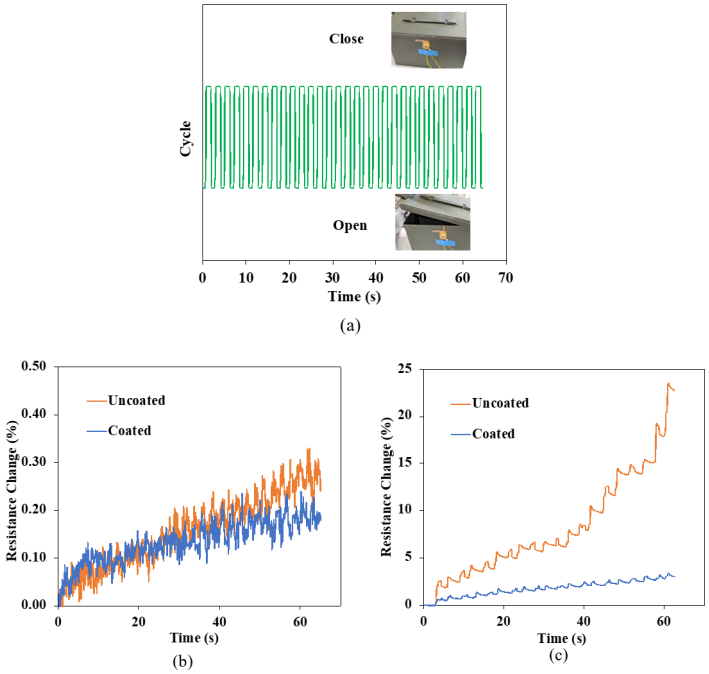

Figure 13: (a) 30 cycles opening and closing the container lid, resistance changes of the (b) CFS, and (c) PFS while opening and closing the container lid.

In elongation test, the stress versus strain graphs for CFS and elongated samples with encapsulant coating layer are shown in [Fig. 14(a) and (b)]. In each test, the test coupon was elongated until it breaks, and the force required to break/tear the test coupon was recorded. An average stress of 121.10 ± 1.20 MPa and 83.40 ± 2.30 MPa was measured to break/tear the CFS and PFS test coupons respectively. Furthermore, a Young's modulus of 7.17 GPa and 2.6 GPa was calculated from linear the region of the stress-strain characteristic curves of CFS and PFS test coupons, respectively. In addition, the results of PFS samples with and without Chemtronics® CTFC-12 did not exhibit a meaningful difference between the stress-strain curves of the coated and uncoated layers.

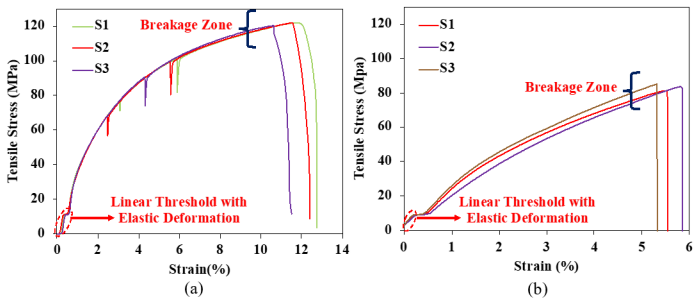

Figure 14: Elongation test: stress-strain curves of (a) CFS, and (b) PFS.

In bending test, during each cycle, both CFS and PFS samples demonstrated minimal average resistance changes, with CFS showing a change of approximately 0% when transitioning from an idle to a bend status, and PFS registering a slight 0.1% change under similar conditions. Furthermore, after subjecting the systems to 100 cycles, equivalent to 28 minutes for both CFS and PFS, the resistance response exhibited different behaviors. As shown in Fig. 15(i)(a), CFS maintained a nearly stable response, exhibiting an approximate 2.3% drift between the initial and final cycles. In contrast, PFS sample showed a noticeable increase in resistance, measuring an approximately 6% drift over the same period [Fig. 15(i)(b)]. In addition, SEM micrographs of the printed sample before and after bend test were obtained and are shown in Fig. 15(ii) (c) and (d), respectively.

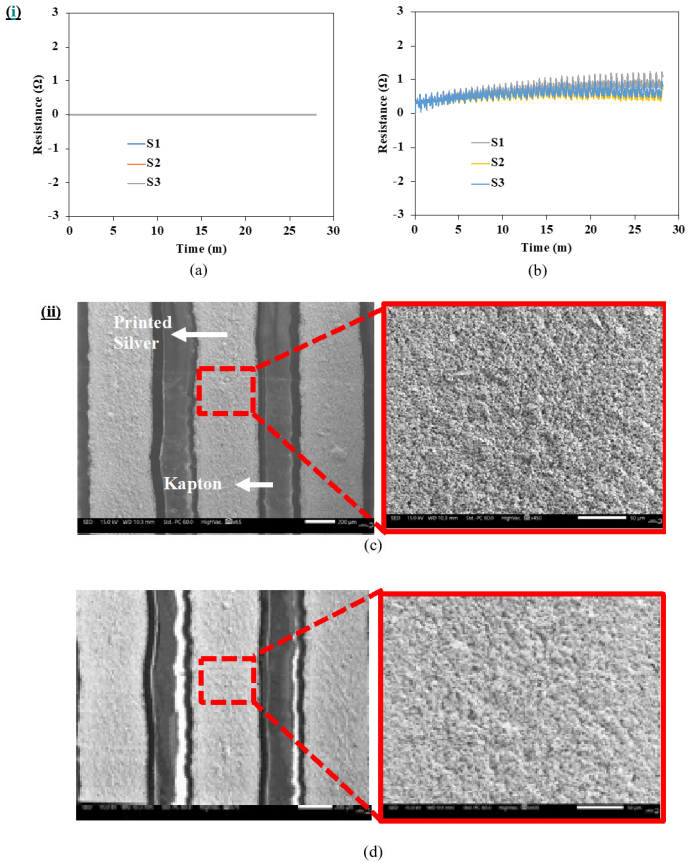

Figure 15: Bend test: (i) resistance response of the test coupon subjected to 180° bend: (a) CFS, and (b) PFS; (ii) SEM micrographs of printed test coupon (c) before bending, and (d) subjected to 180° bend.

In terminal bond strength test, the soldered wire broke/detached from the terminal pad when an average force of 43 N and 3.8 N was applied to CFS and PFS samples, respectively [Fig. 16(i)(a) and (b)].

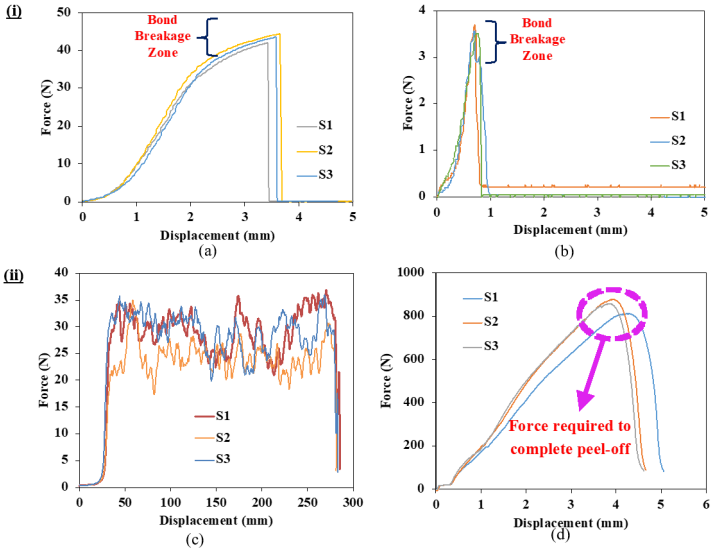

Figure 16: Terminal bond strength test: (i) force required to peel off the wire from (a) CFS, and (b) PFS; (ii) peel test: force required to peel off (c) Kapton®, and (d) ABS from ammunition container stripes with adhesive.

In peel test, shown in Fig. 16(ii)(c), an average force of 25 N was required to completely remove the adhesive and polyimide from the container. This force corresponds to the peeling-off of the temperature sensor on the polyimide interconnect attached to the inside of the ammunition container. Figure 16(ii)(d) shows the direction and average of force (750 N) that was required to completely remove the ABS with adhesive from the ammunition container and this force corresponds to peeling off the enclosure attached to the outside of the container.

The environmental and mechanical characterizations as well as reliability tests on both the CFS and PFS were performed based on IPC-TM-650 and ASTM test standards and is summarized in Table 1.

Table 1: Comparison summary of CFS and PFS.

Test	Standard	Measured Parameter	Test Coupons Pattern	CFS		PFS	
				Coated	Uncoated	Coated	Uncoated
Durability	-	Resistance Change (%)	Prototype	0.008	0.011	3	24
Moisture & Insulation Resistance	IPC-TM-650, 2.6.3-H	Resistance Change (%)	Comb	0	60	0	0
Corrosion	ASTM E-595	Weight Gain (%),	Comb & Meander Line	<0.4	<0.4	<0.4	<1.3
		Resistance Change (%)	Meander Line	≈0	≈0	≈0	<400
Elongation	IPC-TM-650, 2.4.18.1	Young's Modulus (Gpa)	Dogbone	7.17	7.17	2.6	2.6
Bending	IPC-TM-650, 2.4.3-1	Resistance Change (%)	Meander Line	0	0	0.1	0.1
Terminal Bond Strength	IPC-TM-650, 2.4.20	Force (N)	Rectangle (30 × 15 mm)	-	43	-	3.6

CONCLUSION

This paper introduces a novel FHE-based solution for continuous monitoring of temperature inside a sealed storage container. Mechanical characterizations, including the durability and terminal bond strength tests were conducted, revealing that the CFS version exhibits superior reliability compared to the PFS. In addition, the elongation tests show a lower Young's Modulus of PFS which is desirable to obtain higher flexibility when compared to the CFS version. Both CFS and PFS with encapsulation layer performed similarly in the moisture and insulation resistance test, bending, corrosion, and peel tests. This clearly shows that PFS can perform similar to the CFS if the terminal bond strength (which depends on the solder paste adhesion with the silver ink on the terminal pad) can be improved by identifying the appropriate solder paste. Overall, the PFS system provides a cost-effective solution, with a total cost of under $20, for monitoring temperature within a DoD-relevant ammunition container. Future work will concentrate on characterizing the humidity sensing capability of the developed CFS and PFS across relative humidity changes, ranging from 10% RH to 90% RH.

AUTHOR CONTRIBUTION

M. Panahi and A. J. Hanson contributed equally. The manuscript was written through contributions of all authors. All authors have given approval to the final version of the manuscript.

ACKNOWLEDGMENT

This material is based on research partially sponsored by Air Force Research Laboratory and NextFlex under Agreement Number FA8650-20-2-5506. The U.S. Government is authorized to reproduce and distribute reprints for Governmental Purposes notwithstanding any copyright notation thereon.

The authors identify several commercial products, the mention of which is necessary for the completeness of this manuscript. However, these mentions should not be construed as an endorsement of those products. In addition, the authors would like to thank Rob Feeman, and Wade Rutkoskie from Tekna Inc. for supporting the enclosure design and fabrication.

REFERENCES

[1] M. Marzencki et al., "Remote health, activity, and asset monitoring with wireless sensor networks," 2011 IEEE 13th International Conference on e-Health Networking, Applications and Services, 2011, pp. 98-101, doi: 10.1109/HEALTH.2011.6026796.

[2] P. M. Hart, "Continuous asset monitoring on the smart grid," 2011 IEEE PES Innovative Smart Grid Technologies, 2011, pp. 1-7, doi: 10.1109/ISGT-Asia.2011.6167132.

[3] H. Niu and S. Jagannathan, "High memory passive RFID tags with multimodal sensor design and application to asset monitoring in-transit," 2013 IEEE International Instrumentation and Measurement Technology Conference (I2MTC), 2013, pp. 1615-1619, doi: 10.1109/I2MTC.2013.6555687.

[4] S. Kulkarni, K. Ashok, F. Lambert and D. Divan, "Asset monitoring using smart sensing and advanced analytics for the distribution network," 2019 North American Power Symposium (NAPS), 2019, pp. 1-6, doi: 10.1109/NAPS46351.2019.9000254.

[5] M. Panahi, S. Masihi, A. Hanson, J. R. Rodriguez-Labra, A. Masihi, D. Maddipatla, B. B Narakathu, D. Lawson, M. Z. Atashbar, "Development of a flexible smart wearable oximeter insole for monitoring SpO2 Levels of diabetics' foot ulcer," in IEEE Journal on Flexible Electronics, doi: 10.1109/JFLEX.2022.3232465.

[6] Y. Lu et al., "Multimodal plant healthcare flexible sensor system," ACS Nano 2020 14 (9), 10966-10975, doi: 10.1021/acsnano.0c03757.

[7] US Food and Drug Administration, Available: https://www.fda.gov/news-events/press-announcements/fda-brief-fda-authorizes-longer-time-refrigerator-storage-thawed-pfizer-biontech-covid-19-vaccine, [Accessed Dec. 1, 2023].

[8] P. Escobedo, M. Bhattacharjee, F. Nikbakhtnasrabadi and R. Dahiya, "Flexible strain and temperature sensing nfc tag for smart food packaging applications," in IEEE Sensors Journal, vol. 21, no. 23, pp. 26406-26414, 1 Dec.1, 2021, doi: 10.1109/JSEN.2021.3100876.

[9] PC 5.8: Temperature and Humidity Monitoring Tag, Available: https://www.nextflex.us/project-call/project-call-5-0/, [Accessed Dec. 1, 2023].

[10] S. Nakata, T. Arie, S. Akita, K. Takei, "wearable, flexible, and multifunctional healthcare device with an ISFET chemical sensor for simultaneous sweat ph and skin temperature monitoring," ACS Sensors 2017 2 (3), 443-448, doi: 10.1021/acssensors.7b00047.

[11] S. Masihi et al., "Development of a flexible tunable and compact microstrip antenna via laser assisted patterning of copper film," in IEEE Sensors Journal, vol. 20, no. 14, pp. 7579-7587, 15 July15, 2020, doi: 10.1109/JSEN.2020.2987318.

[12] S. Masihi et al., "Development of a flexible wireless ECG monitoring device with dry fabric electrodes for wearable applications," IEEE Sensor Journal, doi:10.1109/JSEN.2021.3116215, 2021.

[13] S. Hajian et al., "Humidity sensing properties of halogenated graphene: a comparison of fluorinated graphene and chlorinated graphene," 2020 IEEE International Conference on Flexible and Printable Sensors and Systems (FLEPS), Manchester, UK, 2020, pp. 1-4, doi: 10.1109/FLEPS49123.2020.9239564.

[14] X. Zhang et al., "Printed carbon nanotubes-based flexible resistive humidity sensor", IEEE Sensors Journal, vol. 20(21), pp. 12592-12601, 2020, doi: 10.1109/JSEN.2020.3002951.

[15] A. K. Bose et al., "Highly sensitive screen printed strain gauge for micro-strain detection," 2019 IEEE International Conference on Flexible and Printable Sensors and Systems (FLEPS), Glasgow, UK, 2019, pp. 1-3, doi: 10.1109/FLEPS.2019.8792282.

[16] M. Panahi et al., "A smart wearable oximeter insole for monitoring SpO2 levels of diabetics' foot ulcer," 2022 IEEE International Conference on Flexible and Printable Sensors and Systems (FLEPS), Vienna, Austria, 2022, pp. 1-4, doi: 10.1109/FLEPS53764.2022.9781511.

[17] S. Masihi, et al., "A highly sensitive porous PDMS-based capacitive pressure sensors fabricated on fabric platform for wearable applications," ACS Sens., 6, pp. 938−949, 2021, doi: 10.1021/acssensors.0c02122.

[18] S. G. R. Avuthu, B. B. Narakathu, M. Z. Atashbar, M. Rebros, E. Hrehorova, B. Bazuin, P. D. Fleming, M. K. Joyce, "Printed capacitive based humidity sensors on flexible substrates," Sensor Letters, Vol. 9, 1–3, 2011. doi: 10.1166/sl.2011.1633.

[19] S. Hajian et al., "Flexible Capacitive Humidity Sensor Based on Fluorinated Graphene," IEEE Sensors Conference, pp. 1-4, 2019. doi: 10.1109/SENSORS43011.2019.8956564.

[20] M. Panahi et al., "Investigation of temperature effect on the porosity of a fabric based porous capacitive pressure sensor," IEEE International Conference on Flexible and Printable Sensors and Systems (FLEPS), pp. 1-4, 2020, doi: 10.1109/FLEPS49123.2020.9239439.

[21] M. Panahi et al., "Development of a FHE based temperature and humidity sensing system for asset monitoring applications," 2022 IEEE Sensors, Dallas, TX, USA, 2022, pp. 01-04, doi: 10.1109/SENSORS52175.2022.9967273.

[22] M. Panahi et al., "Flexible hybrid electronics based condition monitoring system for sealed containers," 2023 IEEE International Conference on Flexible and Printable Sensors and Systems (FLEPS), Boston, MA, USA, 2023, pp. 1-4, doi: 10.1109/FLEPS57599.2023.10220372.

[23] International Electrotechnical Commission, "Degrees of protection provided by enclosures (IP Code) - IP67: Dust tight and protected against the effects of temporary immersion in water," in IEC Standard 60529, ed: IEC, 2013.

[24] International Electrotechnical Commission, "Degrees of protection provided by enclosures (IP Code) - IP64: Dust tight and protected against splashing water," in IEC Standard 60529, ed: IEC, 2013.

BIOGRAPHIES

Masoud Panahi is a Research Assistant at the Center for Advanced Smart Sensors and Structures (CASSS), pursuing his Ph.D. degree in Electrical Engineering at Western Michigan University (WMU), Kalamazoo, MI, USA; where he also completed his M.S. degree in 2021. He has also worked as a Teaching Assistant for several semesters at the Department of Electrical and Computer Engineering, WMU. His research interests include machine learning, embedded systems, wearables and biomedical sensors, flexible hybrid electronics, and physiological signal processing. In 2022, he received the All University Graduate Research and Creative Scholar Award from WMU, which can be highlighted among many other awards he received during his M.S. and Ph.D. degree.

Anthony J. Hanson was born in Lowell, Michigan in 1995. He received his B.S. and M.S. in electrical engineering and currently working on his PhD. from Western Michigan University, Kalamazoo, MI. While getting his degree, he was involved with the IEEE student branch. Starting in 2017, he joined as a Research Assistant for the Center for Advance Smart Sensors and Structures (CASSS) at Western Michigan University, Kalamazoo, MI. His research interest includes sensor applications, e-textiles, flexible hybrid electronics, embedded systems, and sensor acquisition methods. Mr. Hanson awards and honors include 2019 Department-Level Graduate Research and Creative Scholars Award, Research Excellence Award, 2023 All-University Graduate Student Teaching Effectiveness Award and graduating from the Lee Honors College.

Dr. Dinesh Maddipatla received his B.E. degree in Electrical and Electronics Engineering from Anna University, India in 2013; the M.Sc. degree in Electrical Engineering from Western Michigan University, USA in 2016 and Ph.D. in Electrical and Computer Engineering (ECE) from Western Michigan University (WMU), USA in 2020. From 2020 to 2023, he was a Postdoctoral Fellow and then worked as a Research Associate with the Center for Advanced Smart Sensors and Structures (CASSS), WMU, USA. He also worked as an Electrical Engineer at Safesense Technologies, LLC, USA from 2020 to 2022. He is currently working as an Assistant

Professor at the ECE department, WMU, USA. He was awarded the Technology Transfer Talent Network (T3N) from the State of Michigan, the All-University Research and Creative Scholar Award, and the Dissertation Completion Fellowship from Western Michigan University. His research interests include all aspects of design, fabrication, and characterization of printed electronics focusing on flexible sensor structures, physical and chemical sensors, gas sensors, energy storage devices (batteries), and lab-on-a-chip sensing systems. He is a reviewer for more than 35 international journals, associated editor for 3 journals, and has published over 130 refereed journal articles and refereed conference proceedings. In addition, he has over 15 patents and invention disclosures. He is a Technical Working Group member for NextFlex, a DoD Funded Consortium for Flexible Hybrid Electronics.

Simin Masihi received her Ph.D. degree from Western Michigan University (WMU), Kalamazoo, MI, USA, in 2022. She is currently a tenure track Assistant Professor with the Department of Electrical and Computer Engineering, WMU. Her research is primarily focused on wearables and health monitoring applications and involves the design and development of electronic devices based on emerging field of flexible hybrid electronics (FHE). These devices can seamlessly integrate into the Internet, and the addition of machine learning capabilities will enable patient monitoring in a less supervised setting. She has a great passion in having a positive influence on people's health and quality of life by making healthcare services more accessible to people all around the world. She works on development of various biosignal acquisition systems such as electrocardiogram (ECG), Pulse Photoplethysmography (PPG), and electroencephalogram (EEG). She also works on haptic systems and robotic-assisted medical systems for rehabilitation applications. Her research has resulted in over 40 peer reviewed prestigious journal publications, international proceedings, intellectual property disclosures, and patent applications, and has been featured in various news media such as The Academic Times, AZoSensors, and the SCIENMAG Science Magazine. Masihi is a member of the Institute of Electrical and Electronics Engineers (IEEE) and the American Heart Association (AHA).

Dr. Binu B. Narakathu received the B.E. degree in Electronics and Communication Engineering from Visvesvaraya Technological University, Bengaluru, India; the M.Sc. degree in Computer Engineering from Western Michigan University, USA, in 2009; and the Ph.D. degree from the Department of Electrical and Computer Engineering, at Western Michigan University, USA in 2014. From 2015 to 2017, he was a Post-Doctoral Research Fellow with the Sensor Technology Laboratory (STL), Department of Electrical and Computer Engineering, Western Michigan University, USA. From 2017 to 2019, Dr. Narakathu was a Research Associate in the Center for Advanced Smart Sensors and Structures (CASSS), Department of Electrical and Computer Engineering, Western Michigan University, USA. He is currently an Adjunct Professor in the Department of Electrical and Computer Engineering, Western Michigan University, USA. Dr. Narakathu is also the Co-Founder and President of SafeSense Technologies, a company providing innovative sensor technology solutions for the consumer and defense markets. He has authored over 160 peer-reviewed journal and conference publications. Dr. Narakathu has been granted 7 patents and published more than 30 invention disclosures. His research interests include all aspects of design, fabrication and characterization of flexible hybrid electronics (FHE) based sensors and sensing systems integrating microfluidics, lab-on-chip systems, bio-chemical sensors, bio-electronics, and bio-MEMS devices.

Dr. Bradley J. Bazuin is currently the Chair and a Professor of Electrical and Computer Engineering with Western Michigan University, Kalamazoo, MI, USA. His current research interests include printed electronics, hybrid flexible electronic, wearable medical electronics systems, embedded signal processing, and advanced digital signal processing. He is a founding member of the WMU's Center for the Advancement of Printed Electronics (CAPE) and the Center for Smart Sensors, and Structures (CASSS). Dr. Bazuin earned his B.S. degree in Electrical Engineering from Yale University and M.S. and Ph.D. degrees in Electrical Engineering from Stanford University, Stanford, CA, USA. Before joining WMU, he was a senior systems engineer and principal engineers for nearly twenty years working on wireless communications systems in Sunnyvale, CA.

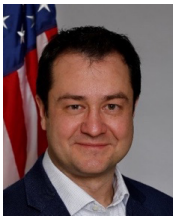

Dr. Scott Miller is the Director of Technology at NextFlex, America's Flexible Hybrid Electronics (FHE) Manufacturing Institute. Dr. Miller is responsible for the portfolio of technical projects funded by NextFlex, its Technical Council and Technical Working Groups, development of FHE industry roadmaps, initiatives within the Institute, and relationships with government, industry, and academic partners. Scott earned his Ph.D. in Chemical Engineering from Princeton University, where he did research on large area electronics manufacturing based on printing processes. Prior to joining NextFlex, Scott led industrial R&D groups in areas including printed, flexible, and hybrid electronics; wearable devices; additive manufacturing; and bioprinting and biofabrication.

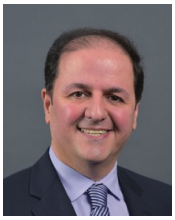

Dr. Massood Z. Atashbar received the B.Sc. degree in electrical engineering from the Isfahan University of Technology, Iran, in 1989, the M.Sc. degree in electrical engineering from the Sharif University of Technology, Iran, in 1992, and the Ph.D. degree from the Department of Communication and Electronic Engineering, Royal Melbourne Institute of Technology University, Melbourne,

Australia, in 1998. From 1998 to 1999, he was a Post-Doctoral Fellow with the Center for Electronic Engineering and Acoustic Materials, Pennsylvania State University, USA. He is currently a Presidential Innovation Professor, Distinguished Faculty Scholar, a Professor of electrical and computer engineering department, and the Founding Director at the Center for Advanced Smart Sensors and Structures (CASSS), Western Michigan University, USA. He has authored or co-authored more than 350 refereed articles, refereed conference proceedings, and four book chapters. In addition, he has more than ten patents and 35 intellectual disclosures. His research interests include physical and chemical sensor development, wireless sensors, energy storage, and nanotechnology applications in sensors and flexible hybrid electronic devices. Dr. Atashbar is a Fellow of IEEE and NextFlex, a DoD Funded Consortium for Flexible Hybrid Electronics. He is currently serving as the Co-Chair of the Technical Working Group for NextFlex.